Anal. Bioanal. Electrochem., Vol. 15, No. 11, 2023, 956-966
https://www.doi.org/10.22034/abec.2023.709112

Analytical & Bioanalytical Electrochemistry

Full Paper

Effect of Reducing Agent on The Electrochemical Performance of The Ag_xO/PVA Nanocomposite

Sakthiraj Kalidoss,[1,*] and Karthikeyan Balasubramanian[2]

[1]*Department of Physics, Kamaraj College of Engineering and Technology, Madurai-625701, Tamil Nadu, India*
[2]*Department of Physics, Mepco Schlenk Engineering College, Sivakasi, Tamil Nadu, 626005, India*

*Corresponding Author, Tel.: +9952353711
E-Mail: shakthiraj.k@gmail.com

Received: 2 March 2023 / Received in revised form: 24 November 2023 / Accepted: 25 November 2023 / Published online: 30 November 2023

Abstract- In the present work, different concentrations of citrate (reducing agent) were used to reduce the silver precursor, and Poly Vinyl Alcohol (PVA) was used as a capping agent. The electrochemical performance of the synthesized multivalent silver oxide (Ag_xO)/PVA nanocomposite has been carefully examined. The well-crystalline, spherical, and aggregate-free Ag_xO/PVA nanocomposite was synthesized. The present findings were strengthened by structural, elemental, and morphological studies. The Ag_xO/PVA nanocomposite showed Surface Plasmon Resonance (SPR) and defect-related band gap mechanisms. The two oxidoreduction peaks in the cyclic voltammogram were observed for the graphite electrode coated with the as-prepared samples. The Ag_xO/PVA-loaded electrodes showed a maximum specific capacitance of 269 Fg^{-1} at a scan rate of 10 mVs^{-1}. It was observed that the citrate can be used to produce silver oxide nanoparticles and to improve the electrochemical functionality of the silver oxide nanoparticles blended with PVA. There are potential uses for this type of nanocomposite-coated electrode in supercapacitors and high-performance energy storage systems.

Keywords- Silver oxide nanocrystal; Poly vinyl alcohol; Electrochemical property; Citrate reduction

1. INTRODUCTION

Due to the combined features of electronic charge transport properties of metal oxide along with the properties of polymeric materials, the polymer blended metal oxide nanocomposites

are receiving a lot of attention. Supercapacitors and other high-power storage devices always require electrodes that have been coated with this kind of nanocomposites [1]. Silver oxide/Poly Vinyl Alcohol (PVA), one of the metal oxide/polymer nanocomposites, is receiving more attention because of its use in antibacterial food packaging [2], plasmonic sensor application [3], surface-enhanced Raman scattering effect [4], and antitumorigenic properties [5]. Among the various preparation techniques available in the literature [6-10], citrate reduction is a straightforward method to control the size of the nanoparticles by adjusting the molar ratio of silver precursors and citrate [11]. The water-soluble, biodegradable PVA has a simple structure with a pendant hydroxyl group. The hydroxyl group of PVA reacts readily with the metal precursor, creating a cross-link between them. The electrochemical studies of the electrodes coated with silver oxide/PVA have received very little attention [12]. The PVA-encapsulated metal-oxide nanoparticles have been reported to be stable for several months and can be stored at room temperature carelessly [13]. The above-mentioned findings made a pathway to the present study towards the investigation of the electrochemical performance of the silver oxide/PVA nanocomposite under different molar ratios of silver precursor ($AgNO_3$) and trisodium citrate.

With silver ions in two different charge states, Ag^{1+} and Ag^{3+}, the silver oxide (AgO) crystallizes in a monoclinic structure [14,15]. So, it is generally described by the $Ag_2^{I}O$-$Ag_2^{III}O$. Due to the presence of interchangeable charge states, this multivalent structure offers a significant oxidoreduction. The focus of this investigation is on how the reducing agent (trisodium citrate) affects the electrochemical performance of the Ag_xO/PVA nanocomposite. In the present study, the chemical reduction method involving citrate is used to synthesize a silver oxide/PVA nanocomposite. The structural, morphological, optical, and electrochemical properties of the as-prepared samples have been analyzed in detail.

2. EXPERIMENTAL SECTION

2.1. Chemicals used

Silver nitrate ($AgNO_3$, ACS reagent, ≥99.0% pure, Sigma Aldrich), Polyvinyl alcohol, (PVA, MW 14,000, Otto Chemie), Trisodium citrate dihydrate ($HOC(COONa)(CH_2COONa)_2 \cdot 2H_2O$, Sigma Aldrich), and ultra-pure water. All the reagents were in analytical grade and used without further purification.

2.2. Synthesis of silver oxide (Ag_xO) / Poly Vinyl Alcohol (PVA) nanocomposite by citrate reduction method

One simple way to control the size of the nanoparticles is to alter the molar ratio of citrate to the silver precursors during the citrate reduction process [11]. The technique that is being presented in this study is unique among the different methods for citrate reduction [16-18]. Following are the reagent quantities used in this study: 0.1 M silver nitrate, 0.15 M polyvinyl

alcohol (PVA), and 0.04 M trisodium citrate (TSC). Deionized water was separately combined with each reagent, and the mixtures were then magnetically stirred for an hour. The PVA solution was then gradually added while stirring the silver nitrate solution. In an aqueous solution, the biodegradable PVA molecules react with the metal salts to form chelates with the metal cations. The temperature was held at 50°C throughout this procedure. Two equal batches of the final reaction mixture were created (Batch 1 & 2). The trisodium citrate solution was then loaded into the micropipette and slowly added to each reaction mixture separately. Trisodium citrate was added twice as much to the batch 2 mixture as it was to the batch 1 mixture. After continuing to stir for two hours, the samples were moved to the oven, and they were heated for two hours at 150 °C. The final solutions were formed in a brownish-black color. For further characterization, the solutions were transferred to the vial. The samples were then referred to as TSC 1 (prepared with low citrate concentration, batch 1) and TSC 2 (prepared with high citrate concentration, batch 2).

2.3. Characterization

X-ray diffraction (XRD) was used to determine the phase structure of the samples using Bruker D8 Advance diffractometer with a Cu-K_α wavelength of 1.5406 Å in the 2θ range from 10° to 80°. The samples' elemental composition, morphology, and particle size were recorded by a CARL ZEISS -SIGMA 300 FESEM with EDAX. The Shimadzu-UV 2450 spectrophotometer was used to record the UV-Vis absorption spectrum. A Thermo Nicolet iS50 - FTIR spectrometer was used to record the Fourier-transformed infrared spectra in the wavenumber range of 400–4000 cm^{-1}.

2.4. Electrode preparation

The 3 mm diameter, 5 cm long, and 99.99% pure cylindrical graphite electrodes were purchased from the market, and the calculated amounts of TSC 1 and TSC 2 nanocomposites were applied on top of them. The Ag_xO/PVA loaded electrodes were then dried in the oven for 5 hours at 100° C.

2.5. Electrochemical measurements

Using an Electrochemical Workstation CHI660C (three electrodes system), all the electrochemical measurements of the synthesized Ag_xO/PVA nanocomposites were made. The working electrode was a graphite rod that had been altered by the as-prepared samples. The counter electrode was made of platinum wire, and the reference electrode was made of Ag/AgCl. In a 0.5 M KOH solution, the electrochemical reaction was carried out. At various scan rates of 5, 7, 9, and 10 mV/s, all the CVs were measured between -0.4 and 0.8 V.

3. RESULTS AND DISCUSSION

3.1. Structural characterization

Using an X-ray diffraction pattern, the composition and structure present in the as-prepared samples were investigated. Using the drop-casting method, the polymer blended nanocomposites were applied to a glass plate and dried for five hours at 100°C. Figure 1 depicts the particle-coated glass plates' X-ray diffraction (XRD) pattern. The pattern reveals that well crystalline mixed valance state of silver oxide formed in the as-prepared samples, and it also blended with the PVA. The (200) plan of reflection from the PVA crystallites is represented by the XRD peak at 22.9° [19,20]. The (111) and (220) crystallographic reflection planes of primitive cubic silver oxide (Ag_2O) (JCPDS card number: 75-1532) are responsible for the peaks at 32.6° and 55.7°, respectively. In addition to that, the X-ray reflections at 2θ of 34.9˚, 42.1˚ and 48˚ can be assigned to the (002), (102), and $(\bar{2}12)$ Monoclinic planes of AgO respectively. (JCPDS card Number: 74-1750). The (111) and (200) reflections from the face-centered cubic silver (Ag) structure (JCPDS card number: 87-0719) are responsible for the reflections at 38.5° and 46.5°, respectively.

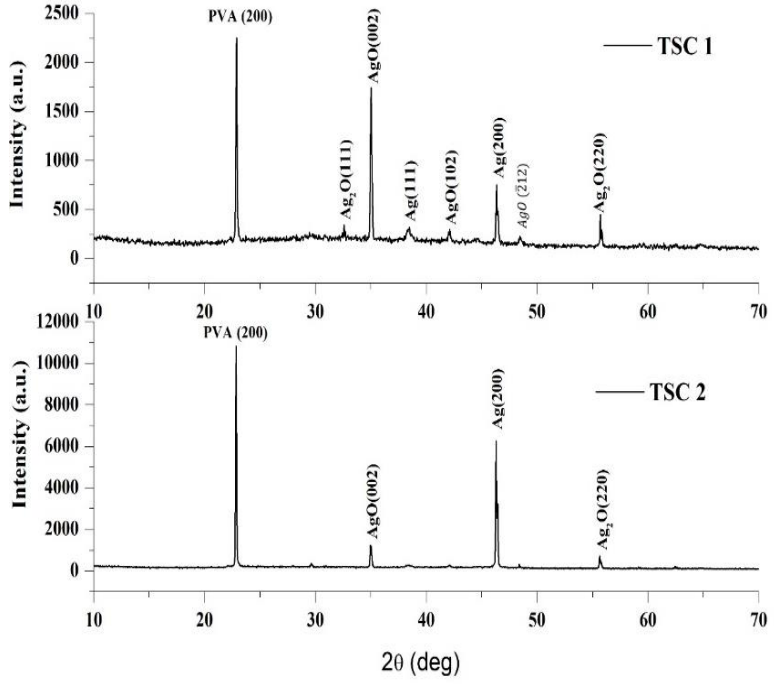

Figure 1. XRD pattern of the Ag_xO/PVA nanocomposite (TSC 1 & TSC 2) coated glass plates

Trisodium citrate (TSC) plays a vital role in the formation of different phases in the crystal [21]. The XRD pattern demonstrates that the crystal growth of cubical silver (Ag) along the (200) plane is significantly increased with increasing TSC concentration. Both samples show the AgO and Ag_2O phases; however, their proportion is high in the samples prepared using low

citrate concentration. This might have occurred because of the presence of active oxygen atoms and hydroxy radicals in the reaction process [22].

3.2. Electron microscopy

The FESEM images were used to evaluate the morphology and size of the samples as prepared. The images of the Ag_xO/PVA sample prepared using low tri-sodium citrate concentration (TSC 1) and high tri-sodium citrate concentration (TSC 2), respectively, are shown in Figures 2(a) and 2(b). The images show that the particles are spherical and evenly distributed throughout the PVA matrix. The TSC 1 specimen contains particles that are about 40 nm in size, while the TSC 2 specimen contains particles that are about 35 nm in size. The increase in tri-sodium citrate concentration increases the pores between the particles. The tri-sodium citrate works well as an anti-aggregation and reducing agent. Therefore, as the citrate concentration is raised, the dispersity of the as-prepared sample increases, opening more space for the effects at the nanoscale.

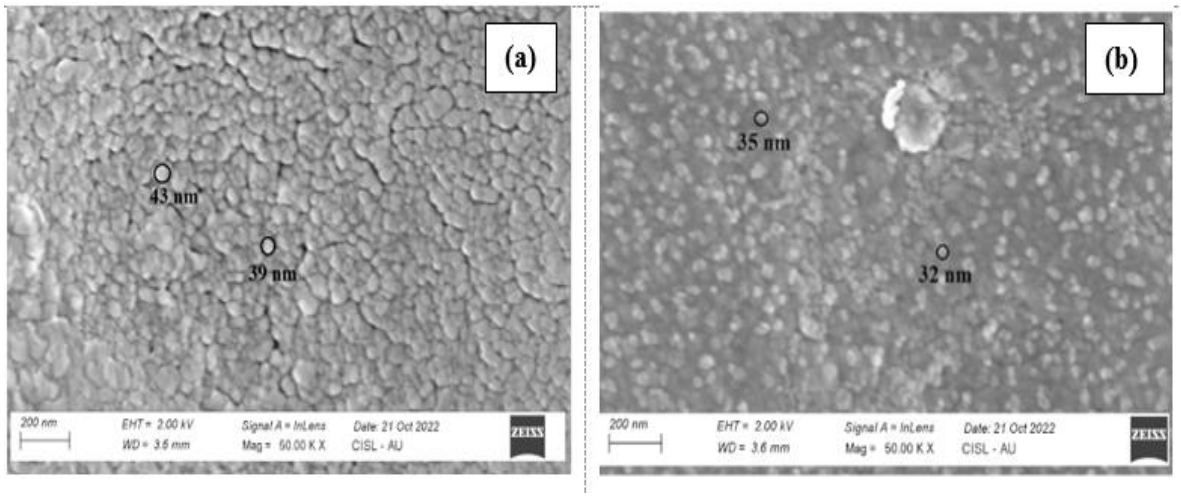

Figure 2. FESEM images of the Ag_xO/PVA nanocomposite were prepared using different tri-sodium citrate concentrations. (a) TSC 1 and (b) TSC 2

3.3. Elemental composition analysis

The EDX spectra, which are depicted in Figure 3, were used to analyse the elemental composition of the samples. The spectra revealed that the peaks for Ag and O are only present in both samples, proving the samples' purity. The inset of the graph contains a table listing the atomic and weight percentages of the elements that were present in the samples. According to the findings, the oxygen percentage decreases as citrate concentration rises.

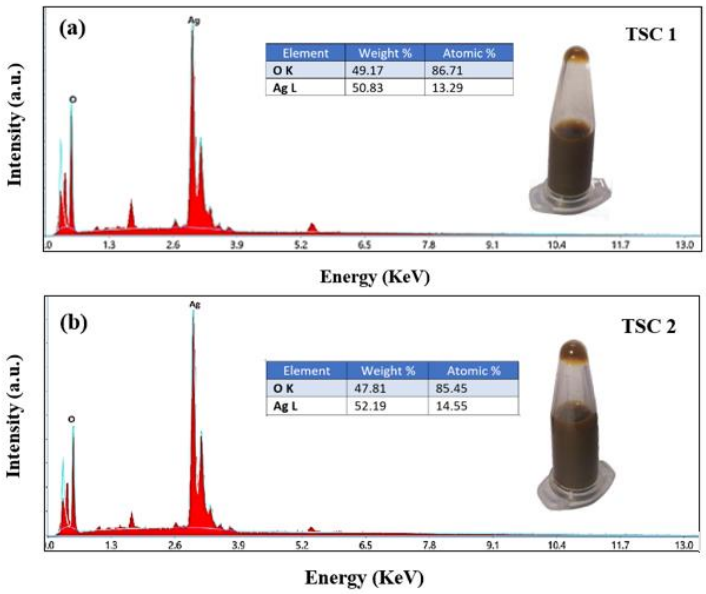

Figure 3. EDX spectra of the (a) sample TSC 1 and (b) TSC 2; the elemental composition chart of the specimen is shown in the inset of the graph.

3.4. Fourier-transformed infrared spectroscopy (FTIR)

Figure 4 displays the FTIR spectra of the liquid phase samples as prepared. The IR absorption patterns in both samples are the same, but their intensities differ significantly. By the band at 3344 cm^{-1}, IR spectroscopy identifies the sample as having a strong O-H stretch [23]. The carbonyl (C=O) stretching mode is indicated by the peak at 1642 cm^{-1} [24]. The small peak at 1346 cm^{-1} is like the CH_2 group's asymmetric C-H bending, confirming the presence of PVA in the samples right after preparation. The strong absorption bands around 600 cm^{-1} and 400 cm^{-1} are attributed to the intrinsic stretching vibration of the metal-oxygen bond [24].

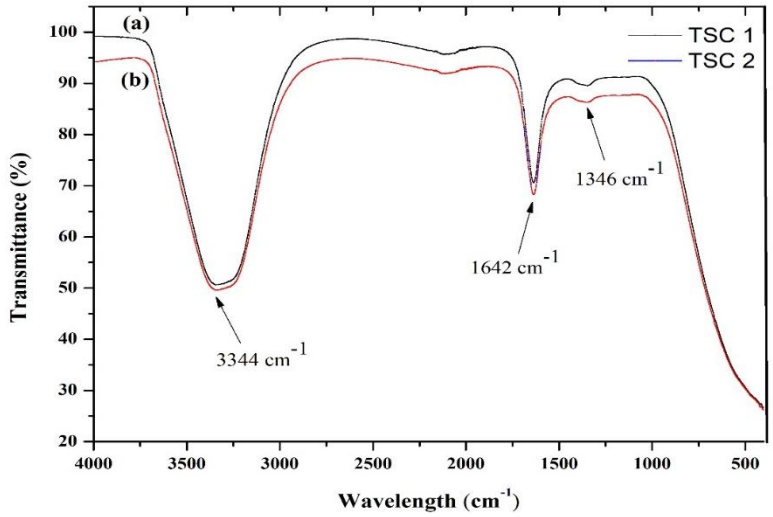

Figure 4. FTIR spectra of the Ag_xO/ PVA nanocomposite (a) TSC 1 and (b) TSC 2

3.5. UV-Vis Spectroscopy

Figure 5 (a) displays the UV-visible absorption spectrum of PVA-blend silver oxide nanocomposites. The strong absorption band with a peak at 438 nm in the violet region is due to the Surface Plasmon Resonance (SPR) of silver nanoparticles [25,26].

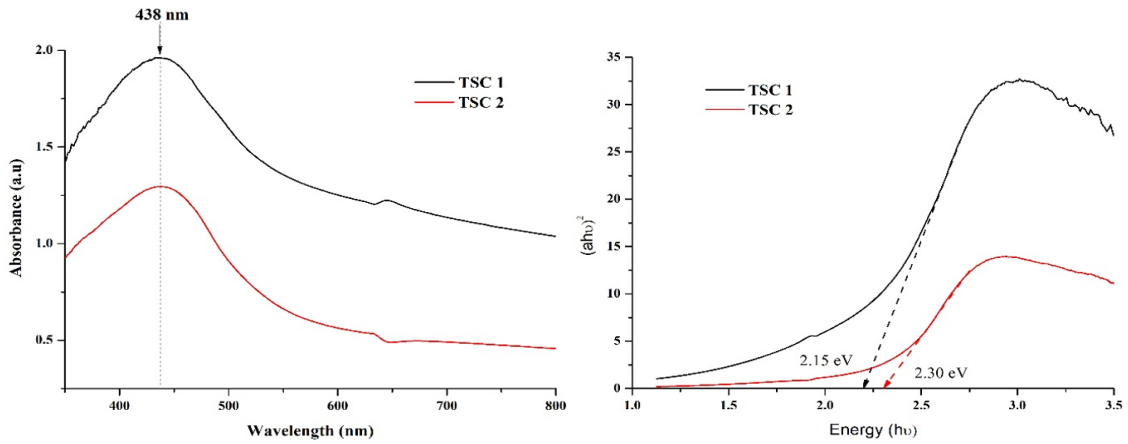

Figure 5. (a) UV-Vis absorption spectra of the Ag_xO/ PVA nanocomposite and (b) Tauc plot of the as-prepared samples

The direct band gap of the samples was calculated using Tauc's relation (Equation 1) from the absorbance data.

$$(\alpha h\nu) = A(h\nu - E_g)^{1/2} \qquad (1)$$

where h is Planck's constant, ν is the photon frequency, and E_g is the optical band gap. Figure 5 (b) shows the Tauc plot of the as-prepared samples.

Ag_2O is an n-type semiconductor with a 1.2–1.5 eV band gap. The calculated direct band gap values for the TSC 1 and TSC 2 samples are 2.15 eV and 2.30 eV, respectively, based on the Tauc relation. The values of the measured band gap agree with those from earlier reports [27,28]. This widening of the band gap from the bulk material is caused by interstitial cations or anion vacancies, whose electrical neutrality is preserved by trapped electrons in their immediate vicinity. The measured band gap values correspond to the visible light wavelength regions and hence it can be concluded that the samples have good photocatalyst properties.

3.6. Electrochemical studies

Cyclic voltammetry (CV) was used to examine the electrochemical performance of the as-prepared samples at a scan rate of 5 mV/s in the potential window of -0.4 to 0.8 V. The results are depicted in Figure 6. It was observed that the prepared electrodes cannot support the higher

scan rates. From Figure 6, it is clear that there are no oxidation or reduction peaks visible on the bare electrode CV curve. Two oxidation (A1 & A2) and two reduction peaks (C1 & C2) can be seen on the sample-coated CV curves. The oxidation peaks A1 peak and A2 peak shift from 0.014V to 0.005V and 0.358V to 0.342V, respectively, as citrate concentration rises. The appearance of peaks A1 and A2 on the anodic side is due to the oxidation of Ag_2O. The observed anodic peaks could be linked to processes such as chemisorption, rapid nucleation of oxide, and ion migration into the microspores as identified in the SEM analysis. The reduction peak C1 moves from 0.278 to 0.251 volts, and the peak C2 moves from 0.595 to 0.619 volts. In comparison to the TSC 1 coated electrode, the electrode modified by sample TSC 2 performs more electrochemically.

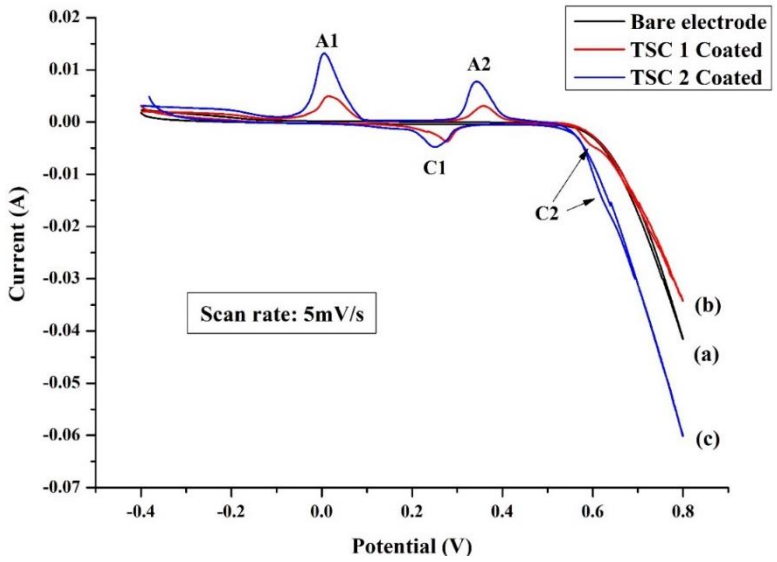

Figure 6. Cyclic voltammogram of the bare graphite electrode (a) and Ag_xO/PVA nanocomposite coated electrodes TSC 1 (b) and TSC 2 (c); the experiment was carried out under the following conditions: Scan rate-5 mV/s, the counter electrode-platinum wire, reference electrode - Ag/AgCl, and electrolyte-0.5 M KOH solution.

The formation of Ag_2O is represented by the oxidation peak (anodic peak) A1, and the formation of AgO is represented by the A2 peak. The reductions of Ag_2O and AgO are represented by peaks C1 and C2, respectively, in the cathodic direction. The earlier reports provide strong support for these findings [29,30].

Figure 7 illustrates how the scan rate affects the sample-coated electrodes in their as-prepared state. As the scan rate is increased, the peak current value rises, demonstrating the electrode's stability. The peak current observed at various voltage levels on both the anodic and cathodic sides of the silver and silver oxide thin films signify pseudo-capacitance behaviour. This indicates the efficient utilization of active electrode material by electrolyte ions during electrochemical reactions.

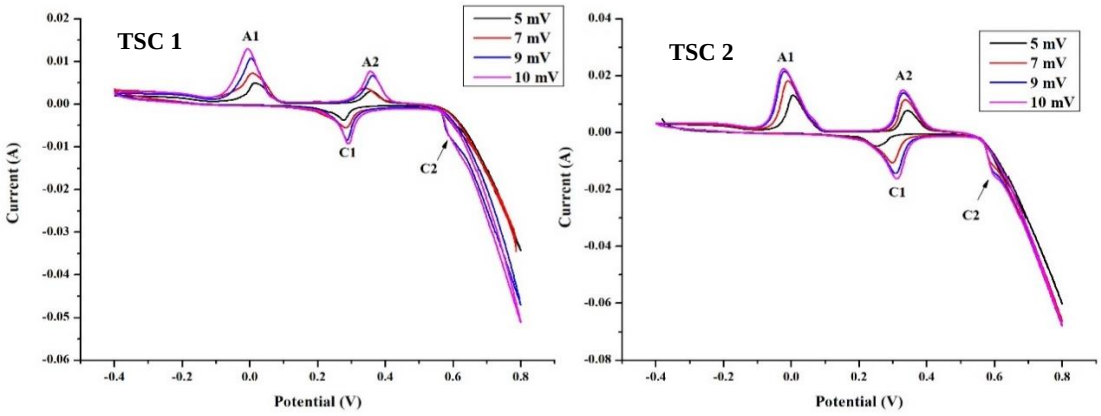

Figure 7. Cyclic voltammogram of the as-prepared sample coated electrode with different scan rates (5mV/s, 7mV/s, 9mV/s & 10mV/s); the experiment was carried out under the following conditions: counter electrode-platinum wire, reference electrode-Ag/AgCl, and electrolyte-0.5 M KOH solution.

Figure 8 displays the variation of the samples' specific capacitance about the scan rate. The graph shows that as the scan rate increases, the specific capacitance value of both samples rises. The specific capacitance of the TSC 2 sample is almost two times greater than that of the TSC 1 sample. TSC 2 sample exhibits a maximum specific capacitance of 269 Fg^{-1} at a scan rate of 10 mVs^{-1}. The elevated capacitance value observed in the TSC 2 sample can be attributed to the presence of more prominent pores and a columnar growth structure. This configuration facilitates improved penetration of the electrolyte, contributing to enhanced performance.

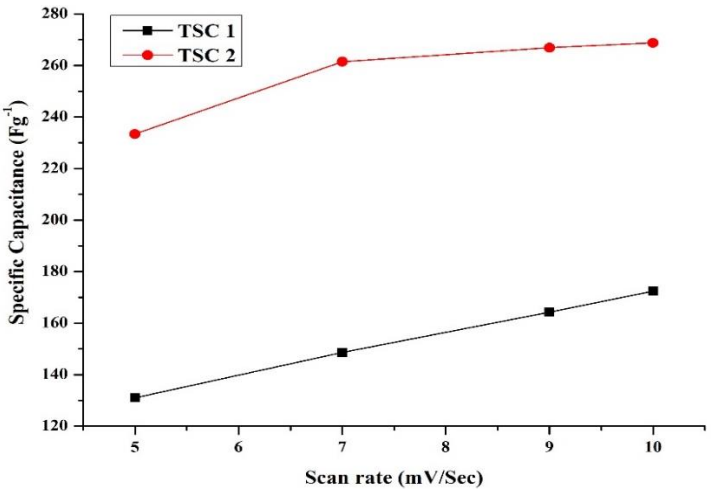

Figure 8. The variation of the specific capacitance value of the as-prepared samples versus scan rate

The supercapacitor performance of the Ag_xO/PVA modified graphite rod was investigated using specific capacitance measured from CV data. The following relation (equation 2) was used to determine the specific capacitance (Cs) of the electrodes as prepared:

$$C_s = \frac{\int I\, dV}{2mk(\Delta V)} \qquad (2)$$

where $(I \times dV)$ is the integrated area under the CV curve, m (g) is the mass of the active material, k (V s^{-1}) is the potential scan rate and ΔV (V) is the potential window.

According to the findings, the electrochemical performance of the electrode is directly influenced by the amount of citrate used in the synthesis reaction. The specific capacitance of the electrode loaded with the sample will double when the citrate concentration is doubled. Therefore, this study offered additional suggestions for refining the reaction parameter settings.

4. CONCLUSION

The straightforward citrate reduction technique was used to successfully synthesize a multivalent nano silver oxide mixture with PVA. Two different citrate concentrations were used to prepare the nanocomposite. The PVA and two silver oxide phases (AgO and Ag_2O) coexisted in the as-prepared samples, according to the XRD pattern. With increasing citrate concentration, the oxygen percentage in the sample decreased. According to the FESEM images, the citrate reduction process produced particles with a size of about 40 nm. Particle sizes were noticeably smaller in nanocomposite materials made with high citrate concentrations. The nanocomposite-modified electrode's cyclic voltammogram demonstrated that the peak current in the electrode rises as the scan rate rises. The sample prepared with a higher citrate concentration has the highest specific capacitance of 269 Fg^{-1} at a rate of 10 mV/s. The electrochemical behaviour in the samples was induced by the formation and reduction of AgO and Ag_2O species, according to the results. The results of the current study suggested that trisodium citrate can control the proportion of Ag and O elements in the samples, allowing one to control the specimen's electrochemical behaviour.

Declarations of interest

The authors declare no conflict of interest in this reported work.

REFERENCES

[1] A. Rose, K. Guru Prasad, T. Sakthivel, V. Gunasekaran, T. Maiyalagan, and T. Vijayakumar, Appl. Surf. Sci. 449 (2018) 551.

[2] S. Pourmoslemi, S. Shokouhi, and R. Mahjub, Packag. Technol. Sci. 34 (2021) 613.

[3] M. I. Skiba, V. I. Vorobyova, and I. V. Kosogina, J. Chem. 2020 (2020).

[4] H. L. Chou, C. M. Wu, F. D. Lin, and J. Rick, AIP Adv. 4 (2014) 087111.

[5] W.R. Rolim, J.C. Pieretti, D.L.S. Renó, B.A. Lima, M.H.M. Nascimento, F.N. Ambrosio, C.B. Lombello, M. Brocchi, A.C.S. de Souza, and A.B. Seabra, ACS Appl. Mater. Interfaces 11 (2019) 6589.

[6] X. Chen, H. Qi, C. Zhang, L. Ma, Z. Li, P. Chen, Q. Xing, Q. Sun, and Z. Yan, Appl.

Phys. A 128 (2022) article id: 374.
[7] J. Xie, R. Wang, Y. Li, Z. Ni, W. Situ, S. Ye, X. Song, Food Chem. 375 (2022) 131708.
[8] A. Farazin, M. Mohammadimehr, A.H. Ghasemi, and H. Naeimi, RSC Adv. 11 (2021) 32775.
[9] B. Behmanesh, D. Rezaei-Ochbelagh, Y. Azizian-Kalandaragh, and G. Imanzadeh-Karkaragh, Curr. Sci. 112 (2017) 735.
[10] E. Karaca, D. Gökcen, N. Ö. Pekmez, and K. Pekmez, Int. J. Energy Res. 44 (2020) 158.
[11] X. Dong, X. Ji, H. Wu, L. Zhao, J. Li, and W. Yang, J. Phys. Chem. C 113 (2009) 6573.
[12] V. Khunseeraksa, S. Kongkaew, P. Thavarungkul, P. Kanatharana, and W. Limbut, Microchim. Acta 187 (2020) 591.
[13] S. Chandran, V. Ravichandran, S. Chandran, J. Chemmanda, and B. Chandarshekar, J. Appl. Res. Technol. 14 (2016) 319.
[14] J.P. Allen, D.O. Scanlon, and G.W. Watson, Phys. Rev. B 81 (2010) 1.
[15] A. N. Mansour, J. Phys. Chem. 94 (1990) 1006.
[16] A. Henglein, and M. Giersig, J. Phys. Chem. B 103 (1999) 44.
[17] Z. Yang, H. Qian, H. Chen, and J. N. Anker, J. Colloid Interface Sci. 352 (2010) 285.
[18] Z.S. Pillai, and P.V. Kamat, J. Phys. Chem. B 108 (2003) 945.
[19] Y.N. Chen, C. Jiao, Y. Zhao, J. Zhang, and H. Wang, ACS Omega 3 (2018) 11788.
[20] S. Gupta, A.K. Pramanik, A. Kailath, T. Mishra, A. Guha, S. Nayar, A. Sinha, Colloids Surf. B 74 (2009) 186.
[21] Q. Zhang, N. Li, J. Goebl, Z. Lu, and Y. Yin, J. Am. Chem. Soc. 133 (2011) 18931.
[22] J. Wei, Y. Lei, H. Jia, J. Cheng, H. Hou, and Z. Zheng, Dalt. Trans. 43 (2014) 11333.
[23] C. Zhang, Q. Yang, N. Zhan, L. Sun, H. Wang, Y. Song, and Y. Li, Colloids Surfaces A 362 (2010) 58.
[24] S. Tripathi, G.K. Mehrotra, and P. K. Dutta, Bull. Mater. Sci. 34 (2011) 29.
[25] S.L. Smitha, K.M. Nissamudeen, D. Philip, and K.G. Gopchandran, Spectrochim. Acta Part A 71 (2008) 186.
[26] L. Mahmudin, E. Suharyadi, A.B.S. Utomo, and K. Abraha, J. Mod. Phys. 6 (2015) 1071.
[27] N.T. Tsendzughul, and A.A. Ogwu, ACS Omega 4 (2019) 16847.
[28] X. Wang, S. Li, H. Yu, J. Yu, and S. Liu, Chem. A Eur. J. 17 (2011) 7777.
[29] R.S. Perkins, B.V. Tilak, B.E. Conway, and H. A. Kozlowska, Electrochim. Acta 17 (1972) 1471.
[30] B.V. Tilak, R.S. Perkins, H.A. Kozlowska, and B.E. Conway, Electrochim. Acta 17 (1972) 1447.